AIAA JOURNAL
Vol. 40, No. 7, July 2002

Scaling Aerooptic Aberrations Produced by High-Subsonic-Mach Shear Layers

Edward J. Fitzgerald* and Eric J. Jumper†
University of Notre Dame, Notre Dame, Indiana 46556

An index-of-refraction model has been shown to produce a reasonable estimate of the aerooptical aberrations measured in a weakly compressible shear layer. This numerical model is a valuable tool both for its insight into the cause of the aberrations and as a source of the parametric data needed to explore and evaluate scaling laws. Scaling relations are developed that describe how the expected aerooptical distortion due to propagation through a free shear layer changes with altitude, that is, static pressure, and/or static temperature. Scaling laws for two cases are developed. In the first case, the Mach numbers of the shear layer's constituent flows are held constant. For the second case, the shear layer's constituent flow velocities are instead held constant. The parametric data are also used to evaluate a scaling law suggested by the literature.

Nomenclature

I	=	maximum far-field irradiance for aberrated system
I_0	=	diffraction-limited, on-axis irradiance
M	=	Mach number
n	=	index of refraction
$\overline{\text{OPL}}$	=	(instantaneous) spatial average optical path length across aperture
p	=	static pressure
q	=	dynamic pressure
R	=	ideal gas constant
$\overline{\text{SR}}$	=	time-averaged Strehl ratio
T	=	temperature
t	=	time
U	=	shear-layer freestream velocity
U_{cn}	=	shear-layer convection velocity, $(U_1 + U_2)/2$
u	=	x-velocity component
v	=	y-velocity component
x	=	streamwise distance
y	=	cross-stream/optical propagation distance
y_1, y_2	=	beam propagation starting, ending points (numerical optics)
γ	=	ratio of specific heats
Δt	=	numerical time step
Δx	=	discrete-vortex numerical method (DVM) vortex convection distance in time Δt
δ_i	=	initial DVM vortex core diameter
λ	=	wavelength of optical beam
ρ	=	density
σ	=	ρ/ρ_{sl}
σ_Φ^2	=	time-/space-averaged optical-phase variance

Subscripts

m	=	known value at a known test condition
new	=	value at desired condition
sl	=	standard day, sea-level condition
0	=	stagnation property
1	=	property of shear-layer high-speed stream
2	=	property of shear-layer low-speed stream
∞	=	freestream property

Superscript

$*$	=	normalized by value at q_∞ of 19.25 kPa

Introduction

THE transmission of a collimated beam of light through a turbulent, variable index-of-refraction flow (caused by temperature or density variations, for example) produces a time-varying, optical distortion on the beam's previously planar wave front. When the depth of the turbulent region is on the same order as the beam aperture or less, the phenomenon is termed "aerooptics."[1] Optical aberrations are typically measured in terms of the variation in the beam's optical path length (OPL) as it traverses the flow. The instantaneous, one-dimensional OPL is defined by[2]

$$\text{OPL}(x,t) = \int_{y_1}^{y_2} n(x,y,t)\,\mathrm{d}y \tag{1}$$

In practice, rather than measuring an absolute OPL, only the relative difference in OPL across the aperture, or optical path difference (OPD), is important. OPD is defined as

$$\text{OPD}(x,t) = \text{OPL}(x,t) - \overline{\text{OPL}}(t) \tag{2}$$

Aerooptical flowfields are usually associated with propagation through turbulent shear and boundary layers. Missiles with optical seekers, airborne telescopes, airborne free-space communication systems, and airborne laser weapon systems, for example, must look through compressible shear and/or boundary layers. For systems like these, aerooptical aberrations translate directly into reductions in system performance. Through the mid-1980s, the design approach was to attempt to estimate the rms degradation and develop a system that could accept these losses.[3] The measure of merit for these systems is the Strehl ratio (SR), defined as

$$\text{SR}(t) = I(t)/I_0 \tag{3}$$

According to the large-aperture approximation, an estimate of the time-averaged $\overline{\text{SR}}$ is given by[4]

$$\overline{\text{SR}} = \exp\left(-\sigma_\Phi^2\right) \tag{4}$$

The phase variance is essentially the normalized OPD variance:

$$\sigma_\Phi^2 \equiv (2\pi\,\text{OPD}_{\text{rms}}/\lambda)^2 \tag{5}$$

The research community is considering the possibility of improving an airborne optical system's performance either by modifying

Presented as Paper 2000-2354 at the AIAA 31st Plasmadynamics and Lasers Meeting, Denver, CO, 19–22 June 2000; received 11 April 2001; revision received 12 December 2001; accepted for publication 18 December 2001.

*Research Assistant, Hessert Center for Aerospace Research, Department of Aerospace and Mechanical Engineering; currently Propulsion Engineer, The Boeing Company, 13100 Space Center Boulevard, MC HZ1-10, Houston, TX 77059-3556. Senior Member AIAA.

†Professor, Hessert Center for Aerospace Research, Department of Aerospace and Mechanical Engineering. Associate Fellow AIAA.

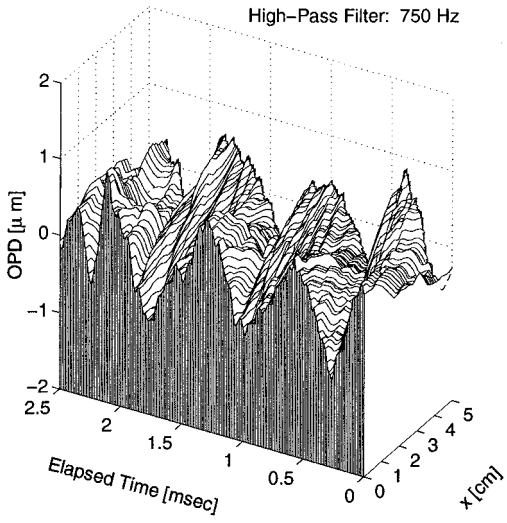

Compressible shear layer[8]

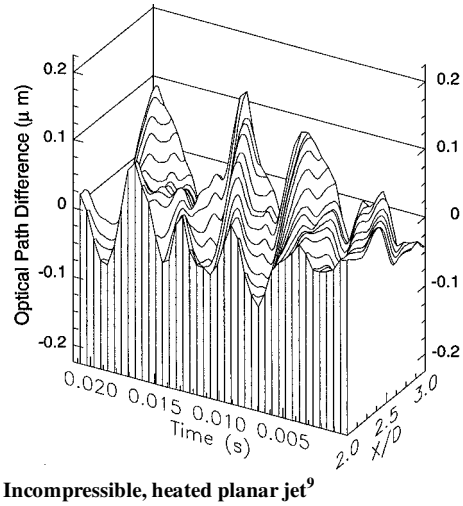

Incompressible, heated planar jet[9]

Fig. 1 Space-time representation of optical wavefront aberrations for two experimental flowfields.

the flowfield to reduce the distortion[5] or by applying a real-time correction using adaptive optics.[6] Practical realities in basic and applied research limit the types and number of ground and flight tests that can be performed to measure aerooptical distortions for a given flight condition. Thus, a means of rationally scaling optical-aberration data obtained at one flight condition to predict the corresponding aberrations (and their spatial and temporal frequencies) at another (untested) condition is clearly of value.

The promise of successful scaling relations was suggested by recently obtained, time-resolved, time-series measurements of optical wave fronts. These wave fronts were produced by a 0.8 Mach, two-dimensional shear layer in a facility located at Arnold Engineering Development Center (AEDC). The measurements were performed by Hugo et al.[7] and were reexamined by the present authors.[8] In both papers, it was found that the compressible shear layer gave rise to wave fronts with coherent-structure-produced peaks and valleys similar to those measured in Hugo and Jumper's 7-m/s heated planar jet[9]; this similarity is clearly seen in Fig. 1. These results suggest that even low-speed, laboratory flow produced optical distortions might be scalable, although the causes of the optical aberrations in the two flows were different. Rather than scaling aberrations produced by the mixing of index-of-refraction mismatched fluids like those of Ref. 9, the present paper considers the scaling of optical aberrations caused by velocity fluctuations in weakly compressible, high-subsonic-Mach flows. Such weakly compressible flows occur on subsonic airborne platforms, for example, where shear-layer convective Mach numbers are typically less than 0.4.

To develop the desired scaling relations, an understanding of the mechanism that creates the optical aberrations is necessary. An analytical/numerical simulation of the AEDC shear layer has been developed by the present authors[8,10] and Fitzgerald[11] and validated at the AEDC conditions by comparison to the experimental results. At the heart of the simulation is a weakly compressible model. This model offered the first rational explanation for the relatively large aberrating fields that would not otherwise have been suspected for such low convective Mach numbers. As described hereafter, this weakly compressible model became a source of the parametric data needed to explore and evaluate scaling laws. The next sections briefly describe the AEDC experiment and the weakly compressible model. Subsequent sections derive and evaluate scaling laws for shear layers where either the Mach numbers or velocities of the constituent flows are held constant while flight altitude is varied.

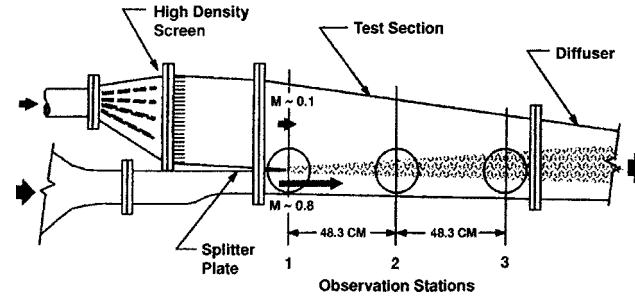

Fig. 2 Schematic of AEDC facility.[12]

AEDC Compressible Shear Layer

The optical wave front measurements in a compressible, two-dimensional, shear layer referred to before were made in the modified Acoustic Research Tunnel located at AEDC.[7] The AEDC shear layer was produced from a ~0.8 Mach high-speed flow mixing with a ~0.1 Mach low-speed flow as shown schematically in Fig. 2. For these tests, the unit Reynolds numbers for the slow and fast streams were 1.4×10^6 and 12.7×10^6/m, respectively. Because each stream was supplied from a common plenum, they shared a common total temperature, $T_0 \approx 27°C$. The static pressure across the shear layer was constant and equal to the stream-matched static pressure, $p_\infty \approx 60.8$ kPa (Ref. 12). These flow conditions can properly be classified as only weakly compressible.[13] Hugo et al.[7] used the small-aperture beam technique[14] to measure wave fronts of an optical beam projected normal to the splitter plate. A more detailed description of the facility is given in Ref. 12.

Weakly Compressible Model

The weakly compressible index-of-refraction model used a discrete-vortex numerical method (DVM) to provide a first-order estimate of the time-varying velocity field. The simulation conditions and optical aperture position corresponded to those of the AEDC facility and station 2 (Fig. 2), respectively. The velocity-field time-series output by the DVM was then used as an input to the weakly compressible model that determined the corresponding density field $\rho(x, y, t)$. The wave front aberrations (OPDs) that would be produced by propagating an optical beam through the instantaneous density, that is, n, fields were then computed.

The weakly compressible model incorporated three mechanisms. An adiabatic heating/cooling mechanism, consistent with Morkovin's strong Reynolds analogy[15] (see also Ref. 13), provided an initial estimate of the instantaneous T and ρ fields. A mechanical balance mechanism was then used to determine the (significant) static pressure fluctuations; that is, the pressure field required to produce the curved streamlines computed by the DVM was determined by iteratively integrating the two-dimensional, unsteady Euler equations:

$$\frac{\partial p}{\partial x} = -\rho\left[\frac{\partial u}{\partial t} + u\frac{\partial u}{\partial x} + v\frac{\partial u}{\partial y}\right] \tag{6}$$

$$\frac{\partial p}{\partial y} = -\rho\left[\frac{\partial v}{\partial t} + u\frac{\partial v}{\partial x} + v\frac{\partial v}{\partial y}\right] \tag{7}$$

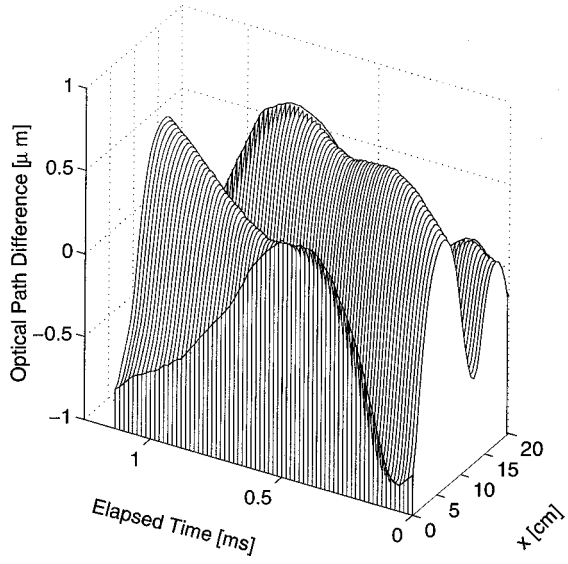

Fig. 3 Optical wavefront aberrations at AEDC conditions (~ 4.115 km, +4°C hot day); weakly compressible model: 20-cm aperture, AEDC station 2, initial $\delta_i/2 = 8.626$ mm.

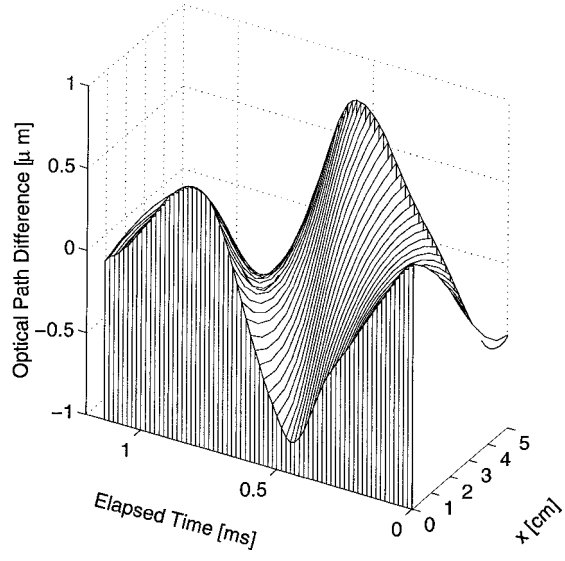

Fig. 4 Optical wavefront aberrations at AEDC conditions (~ 4.115 km, +4°C hot day); weakly compressible model: 5-cm aperture, AEDC station 2, initial $\delta_i/2 = 8.626$ mm.

Finally, a Rancque–Hilsch total-temperature-separation mechanism was modeled by iterating on the static temperature field based on the $p(x, y, t)$ resulting from the solution of Eqs. (6) and (7). The weakly compressible model is detailed in Refs. 10 and 11. Note that, of the three mechanisms, it was the mechanical-balance mechanism that had been generally neglected in the literature by adaptation of Morkovin's analogy (see Refs. 16 and 17). Significant pressure fluctuations have been measured in a 0.45 Mach jet flow,[18] however, and have been apparent in several numerical studies.[19–22] This mechanism was the key, finally, to presenting a rational explanation for a weakly compressible shear layer's aberrating effects.

The OPDs resulting from the weakly compressible model were in good agreement with those measured at AEDC. The best agreement was obtained for the DVM case run with $\delta_i/2 = 8.626$ mm (corresponding to a splitter-plate turbulent boundary-layer thickness of 14.7 mm). The model's data for this case have been shown to agree closely with the AEDC test data, well within the 12% uncertainty of the test data themselves.[8] The resulting wave fronts for the $\delta_i/2 = 8.626$ mm case are shown for 20- and 5-cm apertures in Figs. 3 and 4, respectively. This case will be used for all weakly compressible model results presented in this paper.

Altitude Scaling: Constant Mach Numbers

Examination of the two-dimensional, compressible Euler equations, Eqs. (6) and (7), suggest the possibility of a linear relationship between the density and the pressure-velocity balance. A simple scaling relation would be to assume a linear relation between the density altitude and the resulting $\mathrm{OPD}_{\mathrm{rms}}$. If this were the case, the rms wave front distortion measured at a known test condition $\mathrm{OPD}_{\mathrm{rms}_m}$ might be scaled to another condition, for example, flight altitude, using a relation of the form

$$\mathrm{OPD}_{\mathrm{rms}_{\mathrm{new}}} = \mathrm{OPD}_{\mathrm{rms}_m}(\rho_{\mathrm{new}}/\rho_m) = \mathrm{OPD}_{\mathrm{rms}_m}(\sigma_{\mathrm{new}}/\sigma_m) \quad (8)$$

Other, equivalent, forms of Eq. (8) can be derived by, for example, incorporating the ideal gas law.

$\mathrm{OPD}_{\mathrm{rms}}$ is normally used for determining overall system performance estimates [cf. Eqs. (4) and (5)]; however, for applications such as assessing adaptive optic-correction requirements, the variation of the instantaneous $\mathrm{OPD}(x)$ with altitude is of interest. Note that the derivation of Eq. (8) made no specific assumptions on the $\mathrm{OPD}_{\mathrm{rms}}$. Therefore, similar derivations could be made for scaling the instantaneous $\mathrm{OPD}(x)$. One such example is

$$\mathrm{OPD}_{\mathrm{new}} = \mathrm{OPD}_m(\sigma_{\mathrm{new}}/\sigma_m) \quad (9)$$

Also note that all temperatures in Eqs. (8) and (9) are static temperatures. For a compressible shear layer where both streams have a common T_0, the individual streams will necessarily have different static temperatures. In the present study, the static temperature of the high-speed stream at each condition was chosen for the purpose of matching density. The rationale for this choice was that the high- speed stream dominates the compressibility effects. In addition, this stream's static temperature at altitude would be that given by standard atmosphere tables, making it the convenient choice for back-of-the-envelope scaling estimates.

As will be shown, the scaling relations given by Eqs. (8) and (9) work extremely well when the desired Mach number is assumed to match the tested Mach number. A different scaling (described later in this paper) will be required if the shear layer's velocity difference is to be maintained but at new flight conditions.

Because the DVM velocity field coupled with the weakly compressible model was able to match the measured AEDC OPD data,[8,10,11] it was assumed that the same numerical approach should predict correct OPD estimates for a weakly compressible shear layer at any other conditions. At each new altitude, new DVM velocity data were generated for the AEDC-tested Mach numbers. That is, U_1 was set based on the standard-day static temperature T_1 for that altitude. T_0 of the two streams then followed from the definition[23]

$$T_0 = T\{1 + [(\gamma - 1)/2]M^2\} \quad (10)$$

with $M = M_1 = 0.8$ and $T = T_1$. Because the flows are total temperature matched, the low-speed freestream temperature T_2 also follows from Eq. (10) with $M = M_2 = 0.1$. To maintain identical Mach conditions for the two streams, the DVM could have been rerun with properly scaled shear-layer velocities U_1 and U_2; however, as will be shown, as long as the Mach numbers remained the same, the DVM velocity field results needed only to be appropriately scaled, rather than having to rerun the DVM code.

Velocity Field Scaling

The velocities of the high-speed streams of the shear layer at the tested AEDC conditions ("measured") and for the desired case at a different altitude and/or temperature are given by

$$U_{1m} = M_{1m}\sqrt{\gamma R T_{1m}} \quad (11)$$

$$U_{1\,\mathrm{new}} = M_{1\,\mathrm{new}}\sqrt{\gamma R T_{1\,\mathrm{new}}} \quad (12)$$

respectively. Ratioing Eqs. (11) and (12) and holding $M_{1\,\mathrm{new}} = M_{1m}$ yields

$$U_{1\,\mathrm{new}}/U_{1m} = \sqrt{T_{1\,\mathrm{new}}/T_{1m}} \quad (13)$$

From Eq. (10), the ratio of static temperatures $T_{1\,\mathrm{new}}/T_{1m}$ is given by

$$\frac{T_{1\,\mathrm{new}}}{T_{1m}} = \left\{\frac{T_{0\,\mathrm{new}}}{1+[(\gamma-1)/2]M_{\mathrm{new}}^2}\right\}\left\{\frac{1+[(\gamma-1)/2]M_m^2}{T_{0m}}\right\} = \frac{T_{0\,\mathrm{new}}}{T_{0m}} \tag{14}$$

where, in this case, $T_{0\,\mathrm{new}}$ and T_{0m} are the total temperatures of the standard day and AEDC conditions (constant altitude), respectively. A similar argument can be made for the velocity U_2. Because both constituent flows are at the same T_0, the entire velocity field at any time step can be scaled using the factor $\sqrt{(T_{1\,\mathrm{new}}/T_{1m})}$. To evaluate the unsteady Euler equations [Eqs. (6) and (7)], however, the proper temporal relations must also be maintained; that is, the DVM's discrete vortices must convect the proper distances between time steps. This leads to a requirement to scale the time step to maintain the original convection distances. The convection distance Δx_m of one of the splitter plate vortices, for example, is given by

$$\Delta x_m = U_{\mathrm{cn}}\,\Delta t_m \tag{15}$$

The scaled time step Δt_{new} would then be given by

$$\Delta t_{\mathrm{new}} = \frac{\Delta x_m}{U_{\mathrm{cn}_{\mathrm{new}}}} = \frac{\Delta x_m}{U_{\mathrm{cn}}\sqrt{T_{1\,\mathrm{new}}/T_{1m}}} = \frac{\Delta t_m}{\sqrt{T_{1\,\mathrm{new}}/T_{1m}}} \tag{16}$$

where Eq. (15) has been used to make the final simplification.

To verify that scaling the DVM velocity field was equivalent to running multiple cases, a test run was performed. The shear layer velocities and time step were scaled by the factor

$$\sqrt{\frac{T_{1\,\mathrm{new}}}{T_{1m}}} = \sqrt{\frac{216.7\mathrm{K}}{265.4\mathrm{K}}} = 0.9036 \tag{17}$$

(required to maintain a 0.8/0.1 Mach shear layer at 12.192 km) using Eqs. (13) and (16). Holding all other parameters constant, a new DVM run was performed for the 12.192-km scaled velocities. The resulting DVM shear layer is compared with an original, AEDC DVM run in Fig. 5 for a common time step. If the velocity-/time-step scaling given by Eqs. (13) and (16) did not hold, the most unstable frequency and evolution of the shear layers would be different; in such a case, one would expect very different shear layers to develop. After 84 time steps (the code began with an undeformed layer at time step number 151), both shear layers have rolled up in exactly the same way. [The total elapsed time for each shear layer differs by the factor given by Eq. (17).] This velocity-field scaling verification study is detailed in Ref. 11.

Altitude Variation Results

The $\mathrm{OPD}_{\mathrm{rms}}$ to be expected for a 0.8/0.1 Mach shear layer at different, standard-day altitudes (standard atmosphere) can now be computed using the weakly compressible model. First, the AEDC DVM velocity results and time steps were appropriately scaled with the temperature ratios corresponding to pressure altitudes between 4.115 km (matching the AEDC freestream pressure) and 12.192 km using Eqs. (13) and (16). (The importance of the time-step scaling will be evident hereafter.) The new velocity results were then used to compute new OPDs using the weakly compressible model to provide the the "true" OPD shown in Fig. 6 as "standard-day conditions." (The difference between standard-day and AEDC conditions at 4.115 km in Fig. 6 is that T_1 for the AEDC experiment was 4°C warmer than standard day at that altitude.[24]) Equation (8) was then used directly on the original AEDC OPDs, yielding the curves in Fig. 6 for the two aperture sizes. A comparison of the true OPDs and Eq. (8) scaling to 12.192 km are also shown in Table 1. Figure 6 and Table 1 illustrate that the simple altitude-scaling relation of Eq. (8) correctly models the reduction in overall wave front distortion expected with increasing altitude (and constant Mach numbers).

An estimate of the corresponding system performance degradations due to these $\mathrm{OPD}_{\mathrm{rms}}$ follows from the large-aperture approximation of the time-averaged SR [Eq. (4)]. The resulting $\overline{\mathrm{SR}}$, given a laser wavelength of $\lambda = 1.315$ μm (the wavelength of the chemical oxygen–iodine laser), is shown in Fig. 7. As expected from the $\mathrm{OPD}_{\mathrm{rms}}$ results of Fig. 6, system performance increases with increasing altitude. The effect of the shear-layer-produced distortion is considerable; at the highest altitude (best case), 25–50% of the system performance, that is, $\overline{\mathrm{SR}}$, has been lost. Note that this should be considered an optimistic estimate of a system's overall performance for at least three reasons. First, it has been shown that the large-aperture approximation can underpredict losses caused by coherent structures.[6] Second, the Rancque–Hilsch mechanism was modeled using an isentropic expansion/compression assumption and tended to reduce the distortion amplitude[10,11]; if this mechanism proved to be less than isentropic, a larger distortion would result.[11] Finally, also note that the $\overline{\mathrm{SR}}$ prediction includes only the effect of propagation through the thin boundary of air over the airborne exit aperture

Table 1 Scaling of $\mathrm{OPD}_{\mathrm{rms}}$ from AEDC to 12.192 km, standard day temperature conditions (AEDC Mach numbers maintained), weakly compressible model results, $\delta_i/2 = 8.626$ mm

Aperture size, cm	$\mathrm{OPD}_{\mathrm{rms}}$ at AEDC conditions, μm	AEDC scaled to 12.192 km by Eq. (8), μm	Numerical solution for 12.192 km, μm	Difference, %
20	0.4509	0.1712	0.1711	0.076
5	0.2943	0.1117	0.1117	0.058

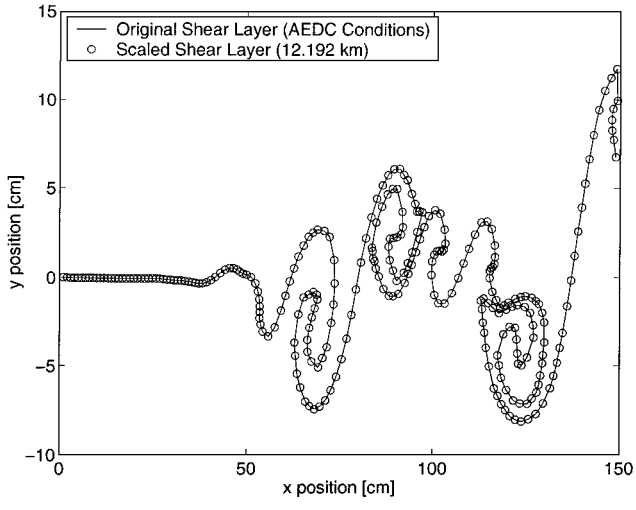

Fig. 5 Effect of scaling shear-layer velocities and time step using Eqs. (13) and (16): loci of DVM discrete vortex positions for constant scaling factor ($M_1 = 0.8$, $M_2 = 0.1$, time step = 235, $\delta_i/2 = 34.5$ mm).

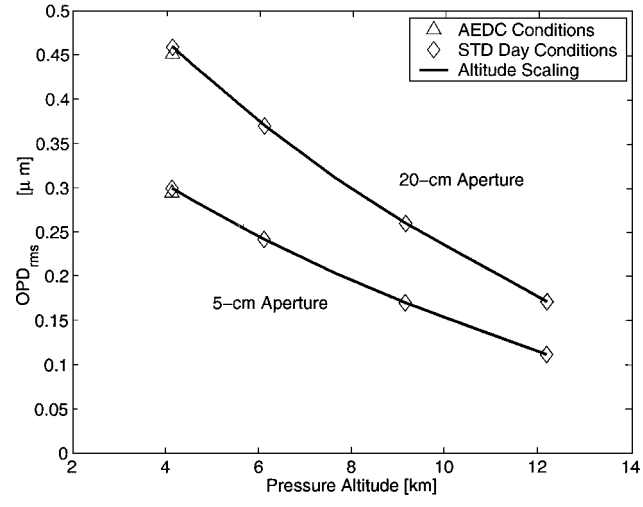

Fig. 6 Effect of altitude on $\mathrm{OPD}_{\mathrm{rms}}$ (Mach numbers fixed) as computed by weakly compressible model (symbols) and using Eq. (8) (lines) (AEDC station 2, $\delta_i/2 = 8.626$ mm).

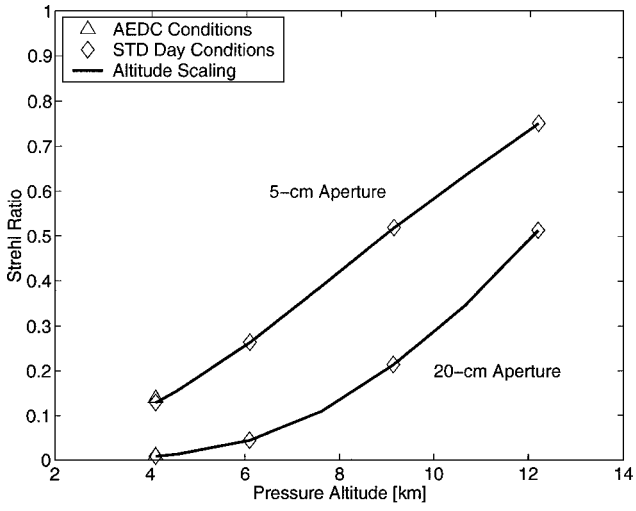

Fig. 7 Effect of altitude on $\overline{\mathrm{SR}}$ for $\lambda = 1.315$-μm light (Mach numbers fixed) as computed by weakly compressible model (symbols) and using Eq. (8) (lines) (AEDC station 2, $\delta_i/2 = 8.626$ mm).

and does not include all contributors to the overall system reduction in $\overline{\mathrm{SR}}$, such as atmospheric turbulence.

The effect of aperture is particularly apparent in Figs. 6 and 7: increasing the aperture from 5 to 20 cm significantly increased the time-averaged OPD with a concomitant 30–90% additional reduction in performance. This suggests that even a fairly crude adaptive-optic (a mirror with four, 5-cm, segments, for example) has the potential for a significant improvement in $\overline{\mathrm{SR}}$.

As noted, because no assumptions have been made about $\mathrm{OPD}_{\mathrm{rms}}$, instantaneous OPDs might also be expected to scale with altitude by the density ratio given in Eq. (9). To test this hypothesis, an individual AEDC-condition wave front was scaled to 12.192-km pressure altitude using Eq. (9) and overlaid on the corresponding wave front computed using the weakly compressible model on the appropriately scaled DVM velocity field (and time step). The result for the two different test apertures is shown in Fig. 8. As was true for the rms wave front distortion, the scaled instantaneous AEDC-condition wave front is in excellent agreement with the wave front computed by the weakly compressible model. This agreement holds for both aperture sizes.

The effect of altitude on the instantaneous wave front distortion can be shown by comparing the results for the AEDC conditions (Figs. 3 and 4) with those computed at 12.192-km pressure altitude using the weakly compressible model on the scaled DVM velocity field/time step (holding Mach constant). The 12.192-km altitude results are shown as waterfall plots in Figs. 9 and 10 for the 20- and 5-cm apertures, respectively. Figures 9 and 10 illustrate that the amplitude of the optical aberration is significantly reduced at high altitude, although the spatial shape of the wave front is largely unchanged. Thus, the designer of an adaptive-optic correction system might expect little change in the wave front's spatial frequency with altitude. The temporal frequencies of the aberrations are also reduced. This latter effect comes through the time-step scaling of Eq. (16) and reflects the velocity reductions required to maintain constant Mach numbers as the speed of sound drops with altitude. If the lower-altitude Mach number were sufficient for the aircraft flight at the design (high) altitude, a significant reduction ($\sim$11%) in adaptive-optic update rate might be realized over that implied by the AEDC test results.

Altitude Scaling: Constant Velocity Difference

In the preceding section, it was assumed that the original AEDC Mach numbers were maintained with increasing altitude. If the velocity difference between the two streams were instead held constant (i.e., DVM velocity fields not changed for altitude), then an increase in altitude would produce a concomitant change in the Mach number of each stream supplying the shear layer. This increase in Mach can be significant ($M_1 = 0.88$ at 12.192 km), so that the density field and the resulting optical aberration might be expected to get worse.

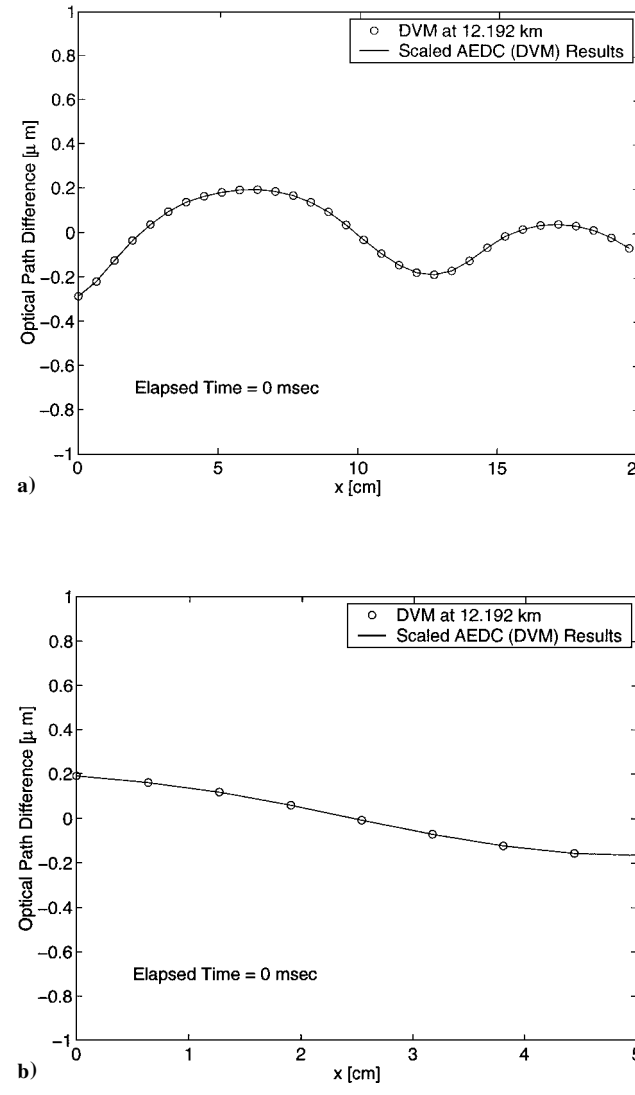

Fig. 8 Comparison of instantaneous optical wave fronts computed at 12.192-km pressure altitude using the weakly compressible model and by scaling results at AEDC conditions using Eq. (9): a) 20-cm aperture and b) 5-cm aperture (constant Mach numbers, AEDC station 2, $\delta_i/2 = 8.626$ mm).

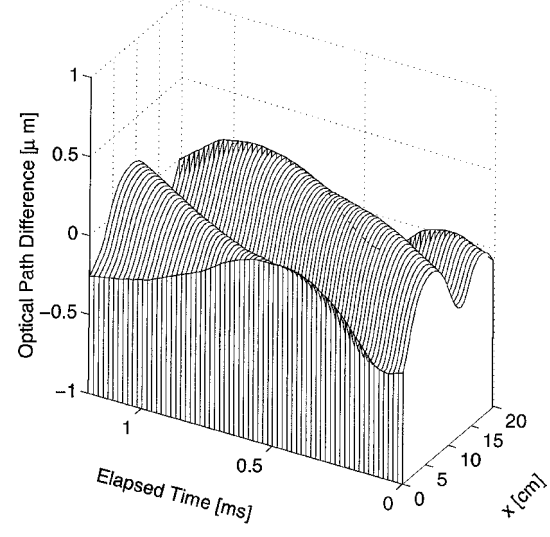

Fig. 9 Optical wave front aberrations at 12.192 km, standard-day conditions (matched Mach numbers); weakly compressible model: 20-cm aperture, AEDC station 2, initial $\delta_i/2 = 8.626$ mm.

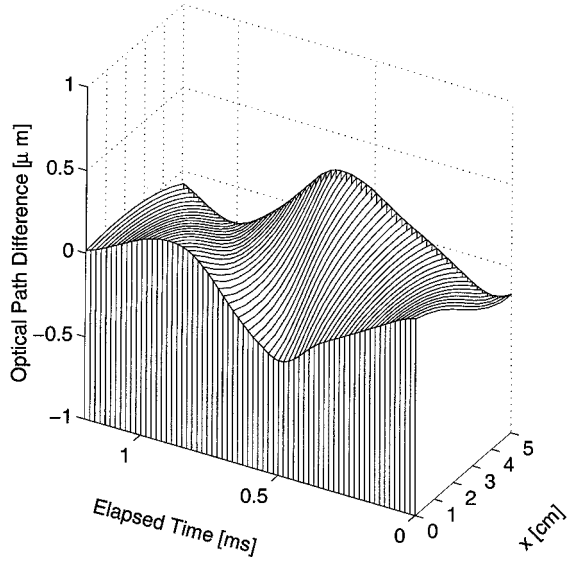

Fig. 10 Optical wave front aberrations at 12.192 km, standard-day conditions (matched Mach numbers); weakly compressible model: 5-cm aperture, AEDC station 2, initial $\delta_i/2 = 8.626$ mm.

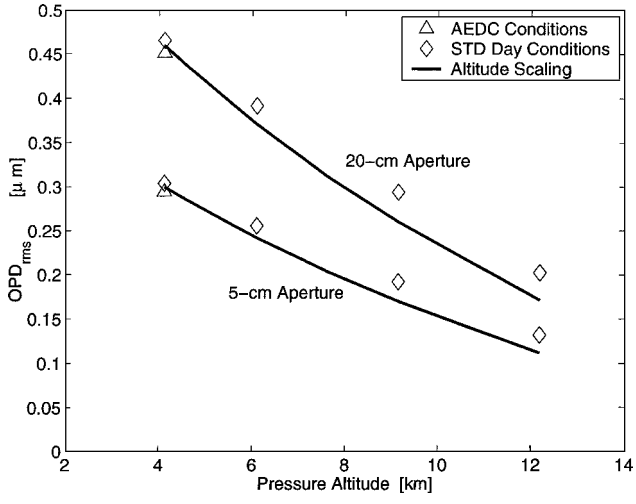

Fig. 11 Effect of altitude on OPD_{rms} (velocity difference fixed) as computed by weakly compressible model (symbols) and using Eq. (8) (lines) (AEDC station 2, $\delta_i/2 = 8.626$ mm).

If the scaling relation of Eq. (8) is applied to this case, the correct trends are still predicted, but the magnitudes of the aberrations are indeed underpredicted, as shown in Fig. 11. Because Eq. (8) has no way to account for the increasing Mach that occurs with altitude, it is no surprise that it underpredicts the additional distortion due to the Mach increase.

The unsteady Euler equations [Eqs. (6) and (7)] again provide insight into what further factor is required to compensate for the underprediction by Eq. (8). If constant Mach numbers are again assumed (for the moment), the velocity/time scaling of Eqs. (15) and (16) can be introduced into Eq. (6) to yield

$$\frac{\partial p}{\partial x} = -\rho\left(\frac{T_{\text{new}}}{T_m}\right)\left[\frac{\partial u_m}{\partial t_m} + u_m\frac{\partial u_m}{\partial x} + v_m\frac{\partial u_m}{\partial y}\right] \tag{18}$$

As demonstrated in the preceding section, the Eq. (8) scaling worked effectively to scale the physics represented by Eq. (18). For the case where the velocity difference is held constant, however, the Euler equation would have a form without the T_{new}/T_m factor:

$$\frac{\partial p}{\partial x} = -\rho\left[\frac{\partial u_m}{\partial t_m} + u_m\frac{\partial u_m}{\partial x} + v_m\frac{\partial u_m}{\partial y}\right] \tag{19}$$

To remove the influence of this temperature ratio, an altitude scaling relation might take the form

$$\text{OPD}_{\text{rms}_{\text{new}}} = \text{OPD}_{\text{rms}_m}(\sigma_{\text{new}}/\sigma_m)(T_m/T_{\text{new}}) \tag{20}$$

As was true for the constant Mach case, no specific assumptions were made on the OPD_{rms} in the derivation of Eq. (20). Therefore, a similar derivation could be made for scaling the instantaneous OPD, namely,

$$\text{OPD}_{\text{new}} = \text{OPD}_m(\sigma_{\text{new}}/\sigma_m)(T_m/T_{\text{new}}) \tag{21}$$

The numerical shear-layer model was again used to test the scaled OPD value, this time using Eq. (20). The true wave front distortion at each altitude condition was again obtained from the weakly compressible index model by changing the input conditions. Unlike the constant Mach case, however, the velocity field and time steps provided by the DVM were kept the same with altitude, producing the same velocity difference. Again, total temperatures were computed using Eq. (10) with $M = M_1$ and T_1 corresponding to pressure altitudes between 4.115 and 12.192 km. The results of the calculations using the weakly compressible model are compared to the scaling law of Eq. (20) in Fig. 12. The results for the 12.192-km case are compared in Table 2. Figure 12 and Table 2 clearly illustrate that the addition of the temperature ratio to the original scaling relation [Eq. (8)] does a reasonable job of predicting this case; however, it is also clear that the new law is less accurate than that for the constant Mach matching of Eq. (8).

The large-aperture-approximated estimate of corresponding system performance degradations due to these OPD_{rms} are shown in Fig. 13. $\overline{\text{SR}}$ follows the same altitude trends as the constant Mach case (cf., Fig. 7) but with an overall reduction in magnitude as would be expected from the higher OPD_{rms} that results when the velocity difference is maintained (cf. Fig. 11). As anticipated, Mach increases translate into larger distortions and additional performance losses.

The 4% difference between the scaled AEDC OPDs and those from the weakly compressible model presented in Table 2 can be traced back to differences in the instantaneous wave fronts. Figure 14 shows comparisons of individual AEDC wave fronts scaled to 12.192-km pressure altitude using Eq. (21) and overlaid on the corresponding wave front computed using the weakly compressible model. As was true for the rms wave front distortion, the scaled

Table 2 Scaling of OPD_{rms} from AEDC to 12.192 km, standard day temperature conditions (AEDC velocity difference maintained), weakly compressible model results, $\delta_i/2 = 8.626$ mm

Aperture size, cm	OPD_{rms} at AEDC conditions, μm	AEDC scaled to 12.192 km by Eq. (20), μm	Numerical solution for 12.192 km, μm	Difference, %
20	0.4509	0.2105	0.2022	4.091
5	0.2943	0.1374	0.1320	4.063

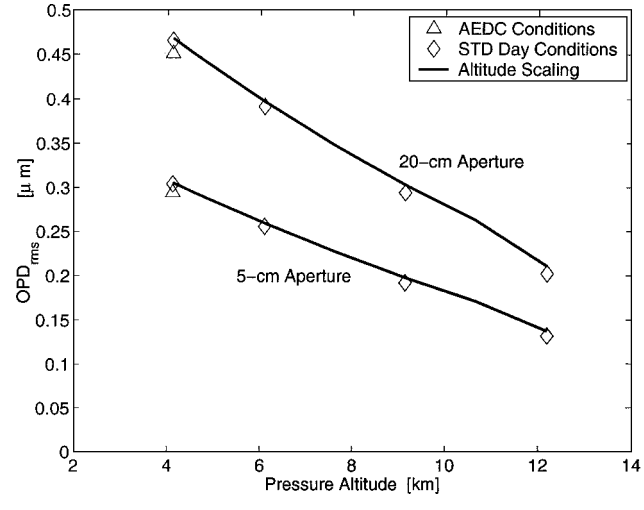

Fig. 12 Effect of altitude on OPD_{rms} (constant velocity difference) as computed by weakly compressible model (symbols) and using Eq. (20) (lines) (AEDC station 2, $\delta_i/2 = 8.626$ mm).

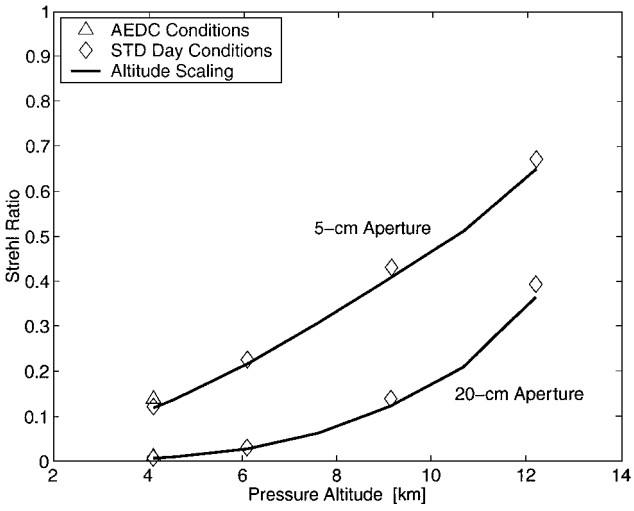

Fig. 13 Effect of altitude on $\overline{SR}$ for $\lambda = 1.315$-μm light (constant velocity difference) as computed by weakly compressible model (symbols) and using Eq. (20) (lines) (AEDC station 2, $\delta_i/2 = 8.626$ mm).

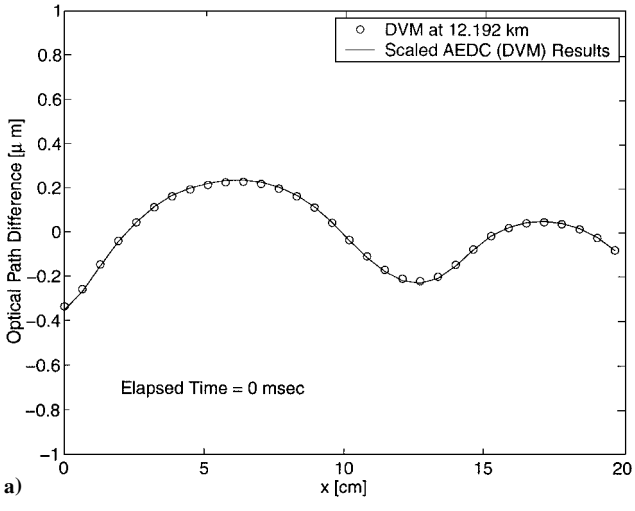

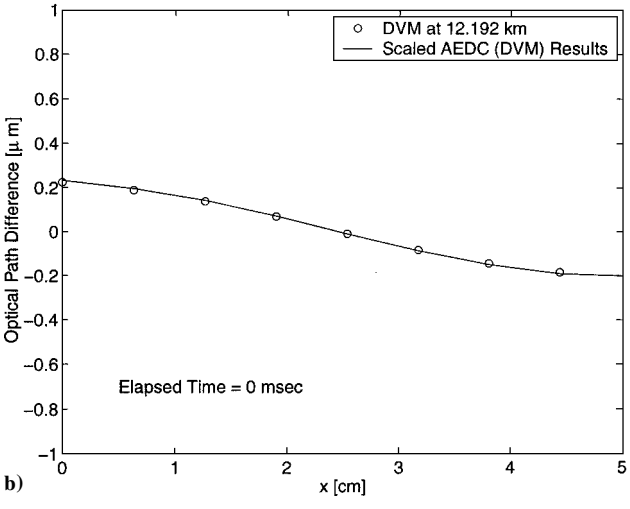

Fig. 14 Comparison of instantaneous optical wave fronts computed at 12.192-km pressure altitude using weakly compressible model and by scaling results at AEDC conditions using Eq. (21): a) 20-cm aperture and b) 5-cm aperture (constant velocity difference, AEDC station 2, $\delta_i/2 = 8.626$ mm).

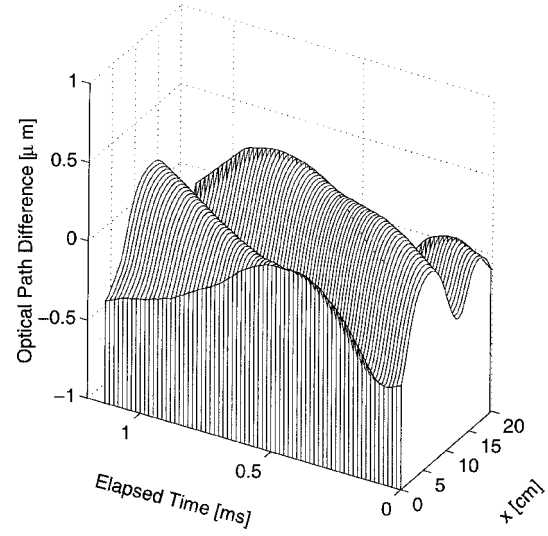

Fig. 15 Optical wave front aberrations at 12.192 km, standard-day conditions (constant velocity difference); weakly compressible model: 20-cm aperture, AEDC station 2, initial $\delta_i/2 = 8.626$ mm.

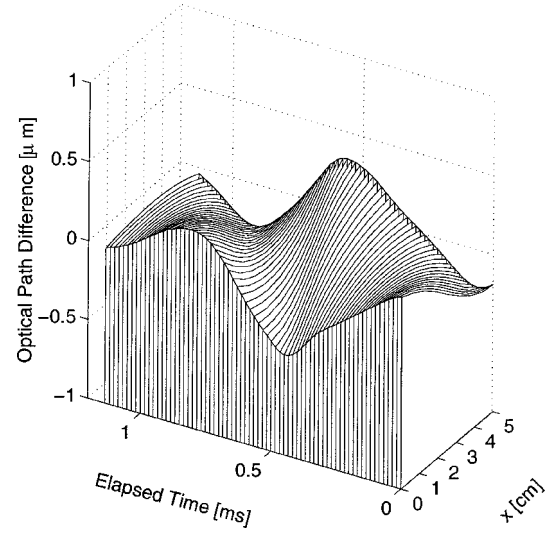

Fig. 16 Optical wave front aberrations at 12.192 km, standard-day conditions (constant velocity difference); weakly compressible model: 5-cm aperture, AEDC station 2, initial $\delta_i/2 = 8.626$ mm.

instantaneous AEDC wave front agrees well with the wave front computed by the weakly compressible model; in fact, the agreement is nearly as good as it was for the constant Mach case (cf. Fig. 8).

The effect of altitude on the instantaneous wave front distortion can be shown by comparing the results for the AEDC conditions with those computed at 12.192-km pressure altitude as shown in Figs. 15 and 16 for the 20- and 5-cm apertures, respectively. Figures 15 and 16 illustrate similar trends as for the constant Mach case. The amplitudes of the optical aberrations are slightly higher for the constant-velocity difference case than they were for the constant Mach case. In contrast to the constant Mach case, the temporal frequencies of the aberrations are unchanged with altitude when the velocity ratio is held constant because no time-step scaling was required. Thus, the designer of a wind-tunnel test of an adaptive-optic correction system might choose the shear-layer velocity ratio to match the flight velocity ratio rather than the flight Mach ratio.

Dynamic Pressure Scaling

The results presented in the preceding two sections can also be used to evaluate the scaling law suggested by Gilbert following a series of KC-135 flight tests.[25] During the tests, a fast-shearing

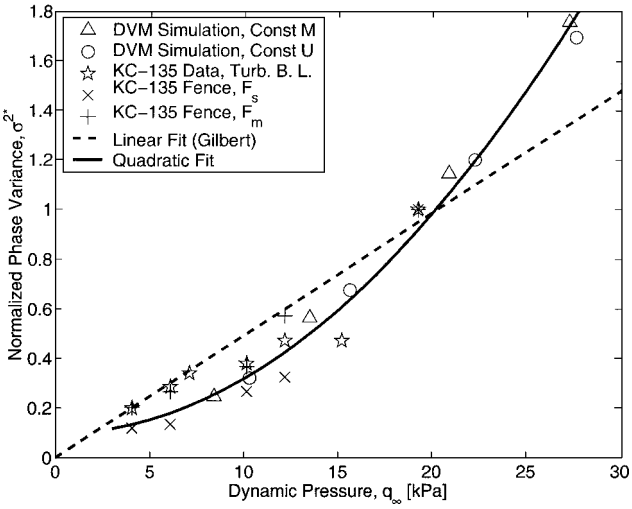

Fig. 17 Effect of dynamic pressure q_∞ on OPD_{rms}; KC-135 data taken from Ref. 25; DVM/weakly compressible model data from AEDC station 2, $\delta_i/2 = 8.626$ mm simulation.

interferometer was used to measure distortions optically. In addition, OPD_{rms} was inferred from hot-wire and laser Doppler velocimeter (LDV) measurements made on the same flights. Data were obtained for three different test configurations. For the first configuration, the distortions were created by the aircraft's (~30 cm thick) turbulent boundary layer. In the second two configurations, upstream, 48% porous fences were used to create turbulent shear layers. The near fence F_s was mounted 8 cm upstream of the optical axis; the second fence F_m was located 80 cm upstream. In comparing phase variances at different flight conditions, Gilbert noted that optical aberrations appeared to increase with increasing dynamic pressure q_∞. To investigate, he normalized the hot-wire/LDV-inferred phase variances for each configuration by the maximum obtained for that test configuration, that is,

$$\sigma^{2*} \equiv \sigma_\Phi^2 \Big/ \left(\sigma_\Phi^2\right)_{\max} \tag{22}$$

The value of $(\sigma_\Phi^2)_{\max}$ also corresponded to the maximum q_∞ obtained during the tests, $q_\infty = 19.25$ kPa (Ref. 25). Gilbert's hot-wire/LDV results are shown with his expected (linear) trend ($\sigma^{2*} = 0.0493 q_\infty/\text{kPa}$) in Fig. 17. Also shown in Fig. 17 are the DVM/weakly compressible model estimates of σ^{2*} for both the constant-Mach and constant-velocity-difference cases. Because the flight conditions examined in the present study reached dynamic pressures significantly larger than those of Gilbert's test, OPD_{rms} was normalized for each case using the appropriate OPD_{rms} for $q_\infty \approx 19.25$ kPa; hence, $\sigma^{2*} > 1$ for several of the points from the DVM/weakly compressible model. The normalized weakly compressible model results show Gilbert's expected trend, falling well within the scatter of his normalized flight-test data.

That the weakly compressible data scales with q_∞ is not surprising because the unsteady Euler equation [Eq. (6)] states that the pressure gradient varies with a density term multiplied by the convective velocity terms (which might be expected to vary as $\sim U_1^2$). As was shown, OPD_{rms} scaled linearly with density, so that one might expect a linear relation between OPD_{rms} and q_∞. For Gilbert's data, such a scaling would be quadratic in q_∞ because σ^{2*} is the normalized square of OPD_{rms}. A better fit of the data, based on the DVM data and the origin, is given by

$$\sigma^{2*} = 0.002222\,(q_\infty/\text{kPa})^2 + 0.09563 \tag{23}$$

and is also shown in Fig. 17. This relation essentially splits the differences between the constant Mach and constant-velocity difference cases. It has the expected quadratic shape, but still has significant uncertainty as shown by the scatter in the data of Fig. 17. [Clearly, Eq. (23) cannot hold near $q_\infty = 0$ because no distortion would exist at this condition.] An unexpected result is that Gilbert's turbulent boundary-layer data (given by the stars in Fig. 17) also follow this relation, that is, within the same scatter range as the shear-layer aberrations. The good overall agreement between the weakly compressible model results and Gilbert's flight-test data strengthens the argument that the weakly compressible model contains the correct mechanisms to explain the aerooptic aberration phenomenon.

Conclusions

The purpose of this study was to develop scaling relations for determining how aerooptical-distortion data obtained for a shear layer at one set of conditions can be scaled to any other altitude, static temperature, or Mach number condition. The weakly compressible model, developed in Refs. 10 and 11 and validated at the single test condition corresponding to the data of Ref. 8, provided a means of testing the validity of candidate scaling relations. These weakly compressible model results were taken as the true results.

Aerooptical distortions were found to scale with a simple density ratio [Eq. (8)] for cases when the Mach numbers of the two constituent flows were unchanged. As a consequence of this, distortion amplitudes decreased with increasing altitude, causing an increase in $\overline{SR}$. Altitude variation changed the instantaneous amplitude of the distortion but not its spatial scales/shapes. The temporal frequencies of the distortion were also reduced (through a rescaled time step) due to the reduction in the constituent flow velocities required to maintain constant Mach with increasing altitude. This suggests that the correction rate required by an adaptive-optic system would reduce by ~10% as altitude increased from 4.115 to 12.192 km.

An additional temperature ratio factor was required to scale aerooptical data collected at one altitude to another for cases where the velocity difference of the constituent flows was held constant [Eq. (20)]. Distortion variation with altitude followed the same trends as for the constant Mach cases; however, distortion amplitudes were larger for the constant-velocity difference cases due to the increase in Mach numbers that accompanies the reduction in the sonic speed with increasing altitude. In this case, wave front temporal frequencies were unaffected by changes in altitude.

The OPD_{rms} data for the weakly compressible model at different altitude conditions were compared to free shear-layer (fence) and turbulent boundary-layer data obtained in actual flight tests by Gilbert.[25] Incredibly, the weakly compressible model data agreed with Gilbert's data to within the experimental measurement uncertainty.

Acknowledgments

These efforts were sponsored by the Air Force Office of Scientific Research, Air Force Material Command, U.S. Air Force, under Grant F49620-97-1-0489. The U.S. Government is authorized to reproduce and distribute reprints for Governmental purposes notwithstanding any copyright notation thereon. The authors would also like to thank D. Kyrazis for his suggestions during this study.

References

[1] Gilbert, K. G., "Overview of Aero-Optics," *Aero-Optical Phenomena*, edited by K. G. Gilbert and L. J. Otten, Vol. 80, Progress in Astronautics and Aeronautics, AIAA, New York, 1982, pp. 1–9.

[2] Klein, M. V., *Optics*, Wiley, New York, 1970, pp. 27, 28.

[3] Jumper, E. J., and Fitzgerald, E. J., "Recent Advances in Aero-Optics," *Progress in Aerospace Sciences*, Vol. 37, No. 3, 2001, pp. 299–339.

[4] Mahajan, V. N., "Strehl Ratio for Aberration in Terms of Their Aberration Variance," *Journal of the Optical Society of America*, Vol. 73, No. 6, 1983, pp. 860–861.

[5] Chew, L., and Christiansen, W., "Coherent Structure Effects on the Optical Performance of Plane Shear Layers," *AIAA Journal*, Vol. 29, No. 1, 1991, pp. 76–80.

[6] Cicchiello, J. M., and Jumper, E. J., "Far-Field Optical Degradation Due to Near-Field Transmission Through a Turbulent Heated Jet," *Applied Optics*, Vol. 36, No. 25, 1997, pp. 6441–6452.

[7] Hugo, R. J., Jumper, E. J., Havener, G., and Stepanek, C., "Time-Resolved Wave Front Measurements Through a Compressible Free Shear Layer," *AIAA Journal*, Vol. 35, No. 4, 1997, pp. 671–677.

[8] Fitzgerald, E. J., and Jumper, E. J., "Aperture Effects on the Aerooptical Distortions Produced by a Compressible Shear Layer," *AIAA Journal*, Vol. 40, No. 2, 2002, pp. 267–275.

[9] Hugo, R. J., and Jumper, E. J., "Experimental Measurement of a Time-Varying Optical Path Difference by the Small-Aperture Beam Technique," *Applied Optics*, Vol. 35, No. 22, 1996, pp. 4436–4447.

[10]Fitzgerald, E. J., and Jumper, E. J., "Further Consideration of Compressibility Effects on Shear-Layer Optical Distortion," AIAA Paper 99-3617, June 1999.

[11]Fitzgerald, E. J., "The Shear Layer Compressibility Mechanism and Its Role in Creating Aero-Optical Distortions," Ph.D. Dissertation, Aerospace and Mechanical Engineering Dept., Univ. of Notre Dame, Notre Dame, IN, April 2000.

[12]Havener, G., and Heltsley, F., "Design Aspects and Preliminary Holographic–Particle Image Velocimetry Measurements for a Subsonic Free Shear-Layer Flow Channel," AIAA Paper 94-2550, June 1994.

[13]Smits, A. J., and Dussauge, J.-P., *Turbulent Shear Layers in Supersonic Flow*, American Institute of Physics, Woodbury, NY, 1996, pp.16–19, 80, 89, 115–131, 133–160.

[14]Jumper, E. J., and Hugo, R. J., "Quantification of Aero-Optical Phase Distortion Using the Small-Aperture Beam Technique," *AIAA Journal*, Vol. 33, No. 11, 1995, pp. 2151–2157.

[15]Morkovin, M. V., "Effects of Compressibility on Turbulent Flows," *Mécanique de la Turbulence*, edited by A. Favre, Centre National de la Recherche Scientifique, Paris, 1962, pp. 367–380.

[16]Rose, W. C., "Measurements of Aerodynamic Parameters Affecting Optical Performance," U.S. Air Force Weapons Lab., TR AFWL-TR-78-191, Kirtland AFB, NM, May 1978.

[17]Rose, W. C., and Johnson, D. A., "Unsteady Density and Velocity Measurements in the 6×6 ft Wind Tunnel," *Aero-Optical Phenomena*, edited by K. G. Gilbert and L. J. Otten, Vol. 80, Progress in Astronautics and Aeronautics, AIAA, New York, 1982, pp. 218–232.

[18]Jones, B. G., Adrian, R. J., Nithianandan, C. K., and Planchon, H. P., Jr., "Spectra of Turbulent Static Pressure Fluctuations in Jet Mixing Layers," *AIAA Journal*, Vol. 17, No. 5, 1979, pp. 449–457.

[19]Sandham, N. D., and Reynolds, W. C., "Three-Dimensional Simulations of Large Eddies in the Compressible Mixing Layer," *Journal of Fluid Mechanics*, Vol. 224, March 1991, pp. 133–158.

[20]Leep, L. J., Dutton, J. C., and Burr, R. F., "Three-Dimensional Simulations of Compressible Mixing Layers: Visualizations and Statistical Analysis," *AIAA Journal*, Vol. 31, No. 11, 1993, pp. 2039–2046.

[21]Chacín, J., and Cantwell, B., "Study of Turbulence Structure Using the Invariants of the Velocity Gradient Tensor," Flow Physics and Computation Div., Dept. of Mechanical Engineering, Rept. TF-70, Stanford Univ., Stanford, CA, Aug. 1997.

[22]Freund, J. B., Lele, S. K., and Moin, P., "Compressibility Effects in a Turbulent Annular Mixing Layer. Part 1. Turbulence and Growth Rate," *Journal of Fluid Mechanics*, Vol. 421, 2000, pp. 229–267.

[23]Anderson, J. D., Jr., *Modern Compressible Flow*, 2nd ed., McGraw–Hill, New York, 1990, p. 59.

[24]AIAA Technical Committee on Design Engineering, *AIAA Aerospace Design Engineers Guide*, AIAA, New York, 1987, pp. 7-6–7-11.

[25]Gilbert, K. G., "KC-135 Aero-Optical Boundary-Layer/Shear-Layer Experiments," *Aero-Optical Phenomena*, edited by K. G. Gilbert and L. J. Otten, Vol. 80, Progress in Astronautics and Aeronautics Series, AIAA, New York, 1982, pp. 306–324.

J. P. Gore
Associate Editor